

# Crack-Path Analysis for Brittle and Non-Brittle Cracks: A Cell Method Approach

E. Ferretti<sup>1</sup>

**Abstract:** Defining the crack path in brittle and non-brittle crack is not easy, due to several unknowns. If the direction of crack propagation can be computed by means of one of the existing criteria, it is not known whether this direction will remain constant during crack propagation. A crack initiation leads to an enhanced stress field at crack tip. During propagation, the enhanced tip stress field propagates into the solid, locally interacting with the pre-existing stress field. This interaction can lead to modifications of the propagation direction, depending on the domain and crack geometry. Moreover, trajectory deviation affects the length of crack propagation. Thus, the length of crack propagation too depends on the domain and crack geometry. Finally, the local interaction between stress fields of opposite signs can return a modified condition of crack arrest. Crack stability analysis cannot be performed without considering this interaction. The problem of defining trajectory deviation, propagation length and crack stabilization is of particular interest in brittle cracks, since these cracks develop statically from the moment of crack initiation forth. It will be shown here how a numerical code for use with the CM returns an accurate crack path for brittle and non-brittle cracks. In both cases, the stress analysis has been performed on the plane of Mohr for each step of the carrying process. At crack propagation, an automatic tool of nodal relaxation with remeshing is used to update the domain geometry.

**keyword:** Cell Method, automatic remeshing, crack stability, failure mechanism analysis.

## 1 Introduction

The Cell Method (CM) is a new numerical method, providing a direct finite formulation of field equations, without requiring a differential formulation [Tonti (2001)]. The first code for application of the CM to Fracture Me-

chanics is due to Ferretti [Ferretti (2001)]. Generalities of this code have been collected in Ferretti (2003a). In particular, it has been shown how the code is able to automatically update the domain geometry as the crack propagates. The updating is achieved by means of a nodal relaxation with intra-element propagation technique. Automatic remeshing is then activated on the new domain, paying attention to refine the mesh on the crack edges. Applications in Mode I and Mixed Mode loading were presented to illustrate the robustness of the implementation. The numerical model incorporates an original tool, which automatically estimates which part of the boundary is subjected to Mode I loading, and which part is subjected to Mode II loading. The tool subsequently estimates the size of the relative displacements between nodes on the opposite sides of the crack surface subjected to Mode II loading, allowing sliding contact to be described. The tool thus represents the CM equivalent of introducing FEM contact elements describing sliding contact [Har (1998), Papadopoulos, Jones and Solberg (1995), Zhong (1995)]. Finally, particular load conditions, with transition from Mode I to Mode II and from Mode II to Mode I as the crack propagates, can also be studied [Ferretti (2003a)]. The tool automatically estimates whether an opened crack re-closes. In this case, the forces transmitted along the re-closed edges are automatically computed from the moment of re-closure forth. The numerical results presented in Ferretti (2003a) show that the CM numerical code can give good predictions for Fracture Mechanics problems. This validates the CM theory for fracture analysis. It has also been shown [Ferretti (2003a), Ferretti (2003b)] how the use of the CM allows us to easily treat multiple domains, internal holes, heterogeneity, singularities on the domain contour, and punctual forces.

Here, the accurateness of the code in describing the crack path is emphasized. In particular, it will be shown how the code is able to take into account crack-induced modifications of the stress field at each step of crack propagation. By means of a crack stability analysis and an ade-

---

<sup>1</sup> DISTART – Scienza delle Costruzioni, Alma Mater Studiorum – University of Bologna, ITALY.

quate criterion for computing the direction of crack propagation, these modifications lead to the identification of a polygonal crack path. The crack stability analysis with updating of the crack propagation direction turned out to be very efficient in describing the crack path.

## 2 Crack Stability Analysis

In crack propagation problems, the geometry of the mesh must be modified as the crack propagates. The ability of the CM code with remeshing to take a general change in the mesh topology easily into account has been shown in Ferretti (2003a). This ability is all the more relevant since changes in mesh topology are rarely supported by classical finite element method (FEM) numerical codes. An example of a remeshing technique can be found in Bouchard et al. (2000).

The remeshing CM code has been implemented in displacement-control. The complete flow-chart for crack propagation analysis and a scheme of the crack geometry updating are given in Fig. 1. As can be seen from Fig. 1, the crack propagation analysis is performed by means of a special element for stress analysis. This element is created as follows, by means of a totally automatic tool:-

- six auxiliary nodes representing the vertexes of a regular hexagon centered on the tip are added to the modeling domain (Fig. 1.b<sub>1</sub>);
- seven new sides, which join the six new nodes and the crack tip node in a counter-clockwise sense, are added to the modeling domain, without crossing the surfaces of the crack (Fig. 1.b<sub>1</sub>);
- a marker is associated with the seven new sides, indicating that the polygon that starts and ends with the crack tip node, and touches all six of the new nodes (Fig. 1.b<sub>1</sub>), is a false hole.

False holes are node chains used to specify smaller or larger elements for particular regions inside the domain. Here, the false hole is used to specify a particular mesh geometry in a region, for use by the mesh generator. This false hole has been termed the “first hexagonal kernel” [Ferretti (2003a)].

The CM uses two meshes, the one the dual of the other. Here, a Delaunay/Voronoi mesh generator [George (1995), Fig. 1.b<sub>1</sub>] is used to generate the two meshes in two-dimensional domains. Once the mesh generator has

been activated, it creates a Delaunay mesh that divides the first hexagonal kernel into five equilateral triangles (Fig. 1.b<sub>1</sub>). This happens because the desired element dimension chosen around the seven vertexes of the first hexagonal kernel is equal to the hexagonal kernel side. The dual mesh (the Voronoi mesh) is formed by the polygons whose vertexes are at the circumcenters of the primal mesh. The Voronoi polygon centered on the crack tip (the gray-shaded polygon shown in Fig. 1.b<sub>1</sub>) has been termed the “crack tip Voronoi cell”. Due to the way it is constructed, four of its sides are positioned equidistant from the crack tip. These sides belong to a hexagon centered on the crack tip, termed the “second hexagonal kernel”.

Since the CM associates geometrical objects of the Voronoi mesh (dual mesh) to source variables, the regularization of the mesh surrounding the tip due to the tip Voronoi cell allows description of the stress field in a finite neighborhood of the tip [Ferretti (2003a)]. The limit analysis for the tip neighborhood has been performed on the Mohr plane. In Fig. 1.b<sub>4</sub>, the Mohr-Coulomb criterion is used to compute the direction of crack propagation.

In plane problems, the crack shape does not vary normal to the plane of the mesh. In this case, the direction of crack propagation will always lie in the plane of the mesh. Then, it is not necessary to construct the complete Mohr’s domain, but only the Mohr’s circle obtained rotating the first hexagonal kernel, since this is the biggest in the Mohr’s domain [Ferretti (2003a)]. Therefore, to obtain the crack propagation direction for the case where the Mohr’s circle is tangent to the limit surface, it is sufficient to calculate the point in the Mohr-Coulomb domain which lies on the limit surface (tangent point). Since the simulation proceeds using finite increments of displacement, it is not possible to capture the precise instant in which the Mohr’s circle becomes tangent to the limit surface. In general, it is only possible to find the first value of displacement for which the Mohr’s circle intersects the limit surface (limit condition). For this case, the tangent point can be found as the point which lies furthest outside the limit surface.

To construct Mohr’s circle, it is sufficient to know any two points in the Mohr-Coulomb plane, and consequently it is sufficient to know the stress field on two attitudes of the same (finite) neighborhood. Since only the sides of the tip Voronoi cell that lie on the second

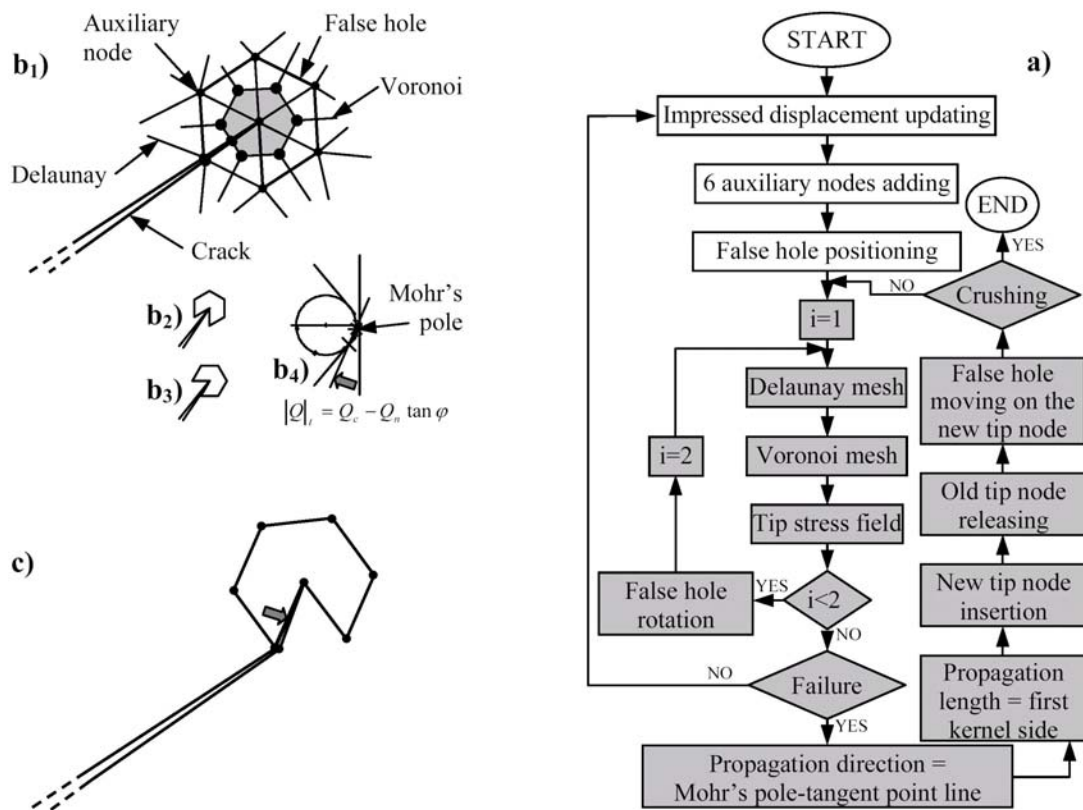


**Figure 1** : a) Flow-chart for crack propagation analysis in displacement-control; b<sub>1</sub>) Scheme of the false hole positioning; b<sub>2</sub>) First orientation of the false hole for analysis in the Mohr-Coulomb plane; b<sub>3</sub>) Second orientation of the false hole for analysis in the Mohr-Coulomb plane; b<sub>4</sub>) Analysis in the Mohr-Coulomb plane and failure criterion; c) Scheme of the false hole moving on the new tip node.

hexagonal kernel need to be taken into account [Ferretti (2003a)], for a general position of the false hole, only three distinct attitudes are available. Of the four sides belonging to the second hexagonal kernel, two are parallel to each other, and correspond to the same attitude. So, one generic position of the false hole is sufficient to identify the circle. Nevertheless, the uncertainty of the false hole orientation cannot guarantee a good accuracy during numerical solution. It has been found [Ferretti (2001)] that the accuracy is not satisfactory for side slopes near to  $0^\circ$  and  $90^\circ$ .

A numerical analysis [Ferretti (2001)] showed that higher accuracy solutions are obtained for side slopes close to  $30^\circ$  and  $60^\circ$ . Since the difference between the slopes of two consecutive sides of the second hexagonal kernel is equal to  $60^\circ$ , it is impossible to insert a false hole giving the higher accuracy solution for at least two sides of the hexagon. Thus, to identify the Mohr's circle, two

different orientations of the false hole can be used. For the first of these (Fig. 1.b<sub>2</sub>), a Voronoi side slope of  $60^\circ$  is available, while for the second (Fig. 1.b<sub>3</sub>), a Voronoi side slope of  $30^\circ$  is available.

Once the limit condition (tangency condition) has been reached, the crack propagation direction is given by the direction of the line that joins the tangent point to the Mohr's pole (Fig. 1.b<sub>4</sub> and Fig. 1.c). The length of crack propagation is assumed equal to the length of the first hexagonal kernel side (Fig. 1.a, Fig. 1.c). This length is one of the inputs of the numerical code. It is fixed by the operator in such a way that the stresses computed on the tip Voronoi cell are stationary. Previous numerical investigations [Ferretti (2001)] show that an upper limit value of the first hexagonal kernel side always exists, for which the stresses on the tip Voronoi cell are stationary. This result is one of the main implications following from the direct discrete stress analysis by means of the CM. The

same result cannot be achieved if a differential formulation or an indirect finite formulation are used. From this point of view, the difference between the CM and other apparently similar methods, such as the finite volume method (FVM), is evident. Actually, even the FVM, which uses integral formulation, is based on a differential formulation. It must be incidentally recalled [Tonti (2001)] that the CM is also very similar to the direct or physical approach initially used in the FEM [Huebner (1975), Livesley (1983) and Fenner (1996)]. The CM can be considered as a generalization of the finite differences method (FDM) as well. However, it was not possible to attain convergence greater than second order both for FVM, physical approach, and FDM. This is the main reason for which the physical approach fell out of favor. The CM (based on a different philosophy) permits the use of interpolation functions, as used in the FEM. This allows the physical approach to be revived. A demonstration of fourth-order convergence with the CM can be found in Cosmi (2000). Details on the differences between variational and discrete formulation can be found in Tonti (2001).

Once the propagation direction has been computed, a new tip node is inserted, the old tip node is relaxed, and the false hole is moved on the new tip node (Fig. 1.a, Fig. 1.c). A special tool has been developed [Ferretti (2003a)] for updating the crack geometry automatically when the limit condition is reached. In Fig. 1.a, the cycle corresponding to the procedure of crack geometry updating for a given value of impressed displacement is the one filled in gray color.

Crack updating is repeated for the same value of impressed displacement until crack stability is achieved (Fig. 1.a). That is, the crack is let to propagate until the condition of no failure at the given impressed displacement is reached. At this point, the value of impressed displacement is incremented and the stress analysis repeated.

In Fig. 1.a, the crushing condition is reached when the specimen is completely cracked. That is, crushing occurs when the dominant crack has divided the specimen into two distinct parts.

### 3 Direction of Crack Propagation

As shown in the former paragraph (Fig. 1.b<sub>4</sub>), the direction of crack propagation is evaluated on the Mohr plane,

by joining tangent point to Mohr's pole. With this choice for the criterion of crack propagation direction, the directions of crack propagation are always two, since two are the tangent points. Nevertheless, the experimental evidence shows that only one crack activates in most cases. It must therefore provide the code with an auxiliary information, in order for the code to be able to answer the question whether one or two cracks activate. In the first case, the code must indicate along which of the two possible directions the crack activates. A way to find the number of activating cracks is to compare the constraint degrees along the two directions to each other. If the constraint degree is the same along both directions, two cracks activate, one for each direction. If the constraint degree along one direction is predominant over the constraint degree along the other direction, only one crack activates. In the latter case, the direction of crack activation is the one along which the degree of constraint (freedom) is minimum (maximum).

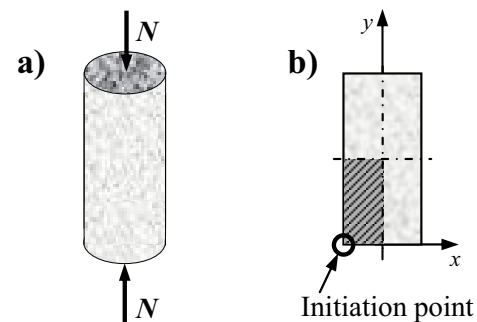


**Figure 2 :** a) Scheme of the compression test on concrete cylinders; b) Modeled domain on the specimen longitudinal section

Degrees of constraint and freedom depend on the single geometry and bond conditions. A simple example can better illustrate the procedure. Consider the case of a cylindrical concrete specimen subjected to mono-axial load [Ferretti (2003a), Fig. 2]. Due to the cylindrical geometry, the problem is plane and no displacements activate orthogonally to the longitudinal section. That is, only Mode I, opening (Fig. 3.a), and Mode II, sliding (Fig. 3.b), are possible on the longitudinal section (Fig. 2b).

The modeled domain is the one marked in Fig. 2b. Reduction of the modeling to only one quarter of the section

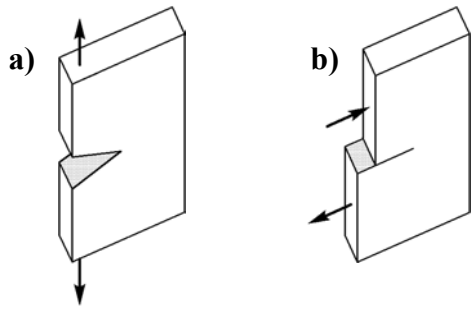


**Figure 3 :** a) Mode I displacements (opening); b) Mode II displacements (sliding)

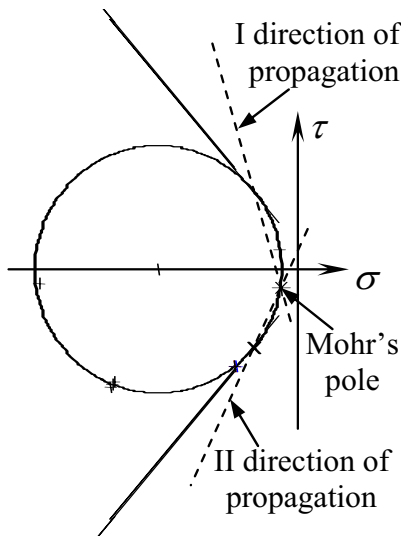


**Figure 4 :** Mohr's circle and directions of propagation for the first propagation step

is possible, due to the double symmetry of the section itself. For the modeled bottom left quarter, the initiation point lies on the bottom platen, and belongs to the cylindrical surface (Fig. 2b). The two directions of crack propagation for the first propagation step are shown in Fig. 4.

As can be appreciated by comparison between Fig. 2b and Fig. 4, for the first step of propagation the crack cannot develop along the first direction of propagation. Since the initiation point belongs to the specimen boundary, indeed, a propagation along the first direction should lead the crack tip to move outside the domain. Thus, for the first step, only the second direction of propagation activates.

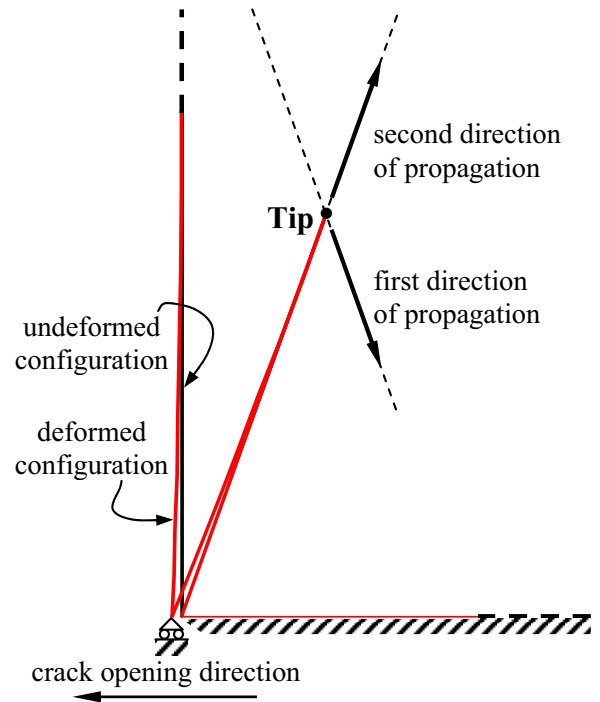


**Figure 5 :** Directions of propagation for an intermediate propagation step

The directions of propagation do not change in the following propagation steps. Mohr's circles similar to the one of first propagation were found for an intermediate step of propagation as well. Thus, the directions of propagation were close to the first and second directions in Fig. 4 for each propagation step. Along these two directions, the constraint degree is not the same. As shown in Fig. 5, opening and sliding displacements along the second direction of propagation are possible for an intermediate propagation step. This happens since the initiation point moves on the bottom platen, giving a crack opening direction which is oblique with respect to the second direction of propagation (Fig. 5). Opening and sliding displacements along the second direction of propagation can therefore occur both for rigid displacements, due to the oblique opening of the crack, and for deformation of the compressed material. On the contrary, opening and sliding displacements along the first direction of propagation can only occur for deformation of the compressed material. This gives to the first direction of propagation a constraint degree greater than the one along the second direction of propagation. Thus, only one crack develops from the tip at an intermediate step of propagation, and

the actual direction of crack propagation is the second. achieved.

## 4 Numerical Crack-Path

### 4.1 Example of Brittle Crack: The Beam in Skew-Symmetric Four-Point Bending

Brittle crack is the term given to static failures caused by crack propagation. It occurs when the crack propagates very rapidly through the material. Such fractures release a lot of energy and can be very loud, explosive and dangerous, as fragments of the material may be cast long distances.

We are faced with a brittle crack whenever the instant of crack initiation is critical for crack propagation. In a load (displacement)-controlled carrying process, this means that, as the crack enucleates, the crack-path develops until crushing with no further need of incrementing the applied load (displacement). Thus, the crack propagation totally occurs for a single value of applied load (displacement), the load (displacement) of crack initiation. The sudden propagation of the crack is caused only by the elastic energy stored in the material (Definition Copyright ©1989 CRC Press LLC).

Brittle crack propagation has been intensely studied in past years. Some examples can be found in Buliga (1999), Hirsch et al. (1992), Holian et al (1997), Ohtsuka (2000), Machida and Aihara (1996), and Kysar (2001).

The difficulty of brittle crack propagation problems consists in the nature of the main unknown: the crack itself, at various moments in time. The research in this field concerns mainly the constitutive behavior of a brittle material. In almost all the studies the geometry of the crack is prescribed. There are a few exceptions, such as the papers of Ohtsuka (2000) or Stumpf and Le (1990). Classical, constitutive oriented theories are useful for the experiments, but they are based on hypotheses which are unrealistic in the case of an elastic structure. Here, the problem of finding the crack configuration at various moments in time has been solved numerically, by means of the CM remeshing code developed in Ferretti (2003a).

At crack initiation, the CM numerical simulation of a brittle failure involves repeating the gray-filled cycle in Fig. 1.a time after time until crushing, since the no propagation condition is never reached for the displacement of crack initiation. That is, the crack never stabilizes for the displacement of crack initiation, and the condition for incrementing the impressed displacement is never

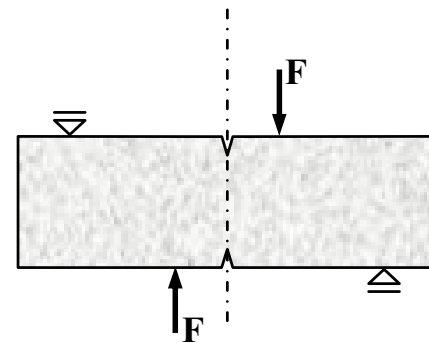


**Figure 6** : Scheme of the skew-symmetric four-point bending test

As an example of brittle crack, consider the beam in skew-symmetric four point bending in Fig. 6. The beam has been pre-cracked at mid-span and a special element for stress analysis has been inserted at both crack tips. The stress analysis for a value of impressed displacement not involving crack propagation is shown in Fig. 7. In this figure, it can be seen how dealing with punctual forces does not represent a problem with the CM. Forces can be directly charged on zones of zero extension (points). This gives a realistic representation of the punching effect in correspondence both of the applied load and the rocker bearings.

The analysis of crack propagation has been performed in displacement-control, in accordance with the flow-chart in Fig. 1.a. From the value of impressed displacement equal to zero up to the displacement of crack initiation, the failure condition is never reached. Thus, crack geometry updating is not required and the value of impressed displacement can be incremented. The tip stress analysis in the Mohr plane for this first stage of the carrying process is shown in Fig. 8. As can be seen from this figure, in the first stage the maximum compressive stresses are neglecting, while the maximum tensile stresses grow rapidly. For the displacement of crack initiation, Mohr's circle is tangent to the limit domain. All Mohr's circles internal to the limit domain represent stable conditions at the given value of impressed displacement. When the circle becomes tangent to the limit domain, a first crack propagation occurs along the directions individuated by Mohr's pole and tangent points. In Fig. 8, only one tangent point has been marked, since only one crack actually

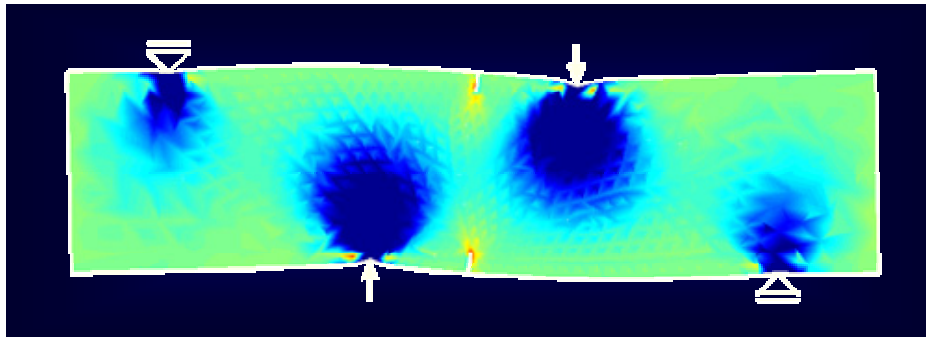


**Figure 7 :** Stress analysis for a value of impressed displacement smaller than the displacement of crack initiation

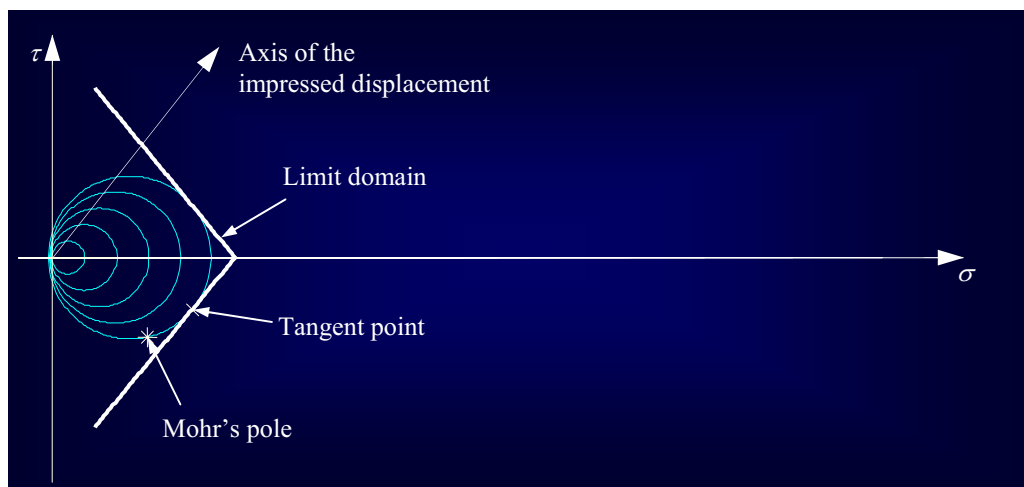


**Figure 8 :** Mohr's circles for tip stress analysis in the first stage of the carrying process

activates, due to a different constraint degree along the two propagation directions. The tangent point marked in Fig. 8 is the actual limit point for the bottom crack tip in Fig. 6.

As regards the length of crack propagation, this is related to the side of the first hexagonal kernel, as previously said. A preventive stress analysis has been performed for a value of impressed displacement smaller than the displacement of crack initiation, by varying the dimension of the first hexagonal kernel. This parametric analysis returned the greater side of the first hexagonal kernel making stationary the stresses on the tip Voronoi cell, generated as previously shown. Stationarity of the stress field with the dimensions of the tip mesh is required in order to guarantee the objectiveness of the performed numerical analysis. Due to geometrical implications (Fig. 1.c), the lower limit for the length of crack propagation in a poly-

gonal crack path is equal to the side of the first hexagonal kernel.

In order to maximize the accurateness in defining the crack path, the length of crack propagation has been fixed equal to its lower limit, the side of the first hexagonal kernel.

After the crack geometry has been updated, a new tip stress analysis is performed for the new tip. In Fig. 9, can be seen how the Mohr's circle corresponding to the tip stress analysis for the first propagation step and the tangent circle are more or less of the same dimensions. By comparison between these two circles, we can also notice that the new circle is shifted along the positive semi-axis of normal stresses with respect to the former one. Shifting along the positive semi-axis of normal stresses leads to circles moving outside the limit domain. Since circles which are outside of the limit domain involve fur-

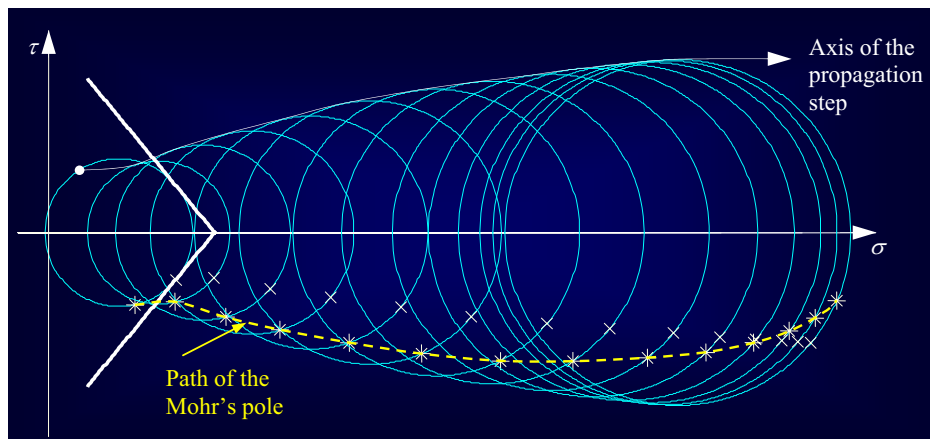


**Figure 9** : Mohr's circles for tip stress analysis in the second stage of the carrying process

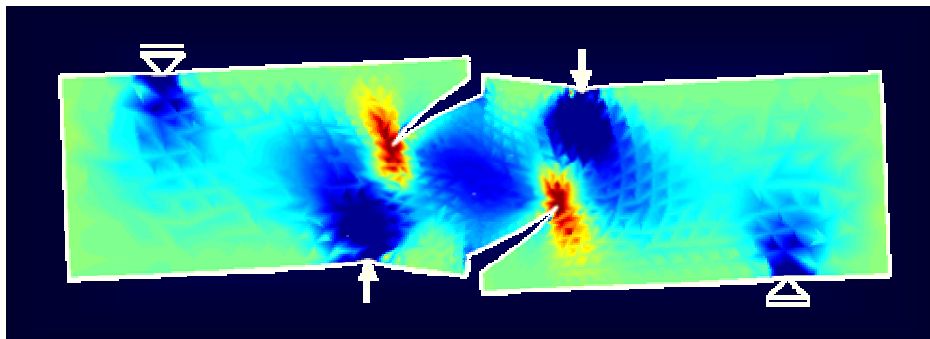


**Figure 10** : Stress analysis after ten propagation steps (second stage)

ther crack propagation, the new condition is not stable. Thus, the condition for going outside the gray-filled cycle in Fig. 1.a is not reached, and a new crack geometry updating is performed for the displacement of crack initiation. This results in a Mohr's circle still shifting along the positive semi-axis of normal stresses (Fig. 9). Crack geometry updating is therefore repeated, in order to reach a stable condition for the displacement of crack initiation, but the amount of shifting becomes greater and greater as the crack propagates (Fig. 9). Moreover, the stress field is locally enhanced by crack propagation, since the radius of the tip Mohr's circle becomes greater and greater as the crack propagates (Fig. 9). Shifting along the positive semi-axis of normal stresses and radius increasing lead the degree of crack instability to grow as the crack propagates at constant value of impressed displacement. This states that the failure which has been activated is actually brittle. The crack propagation steps involving shifting

along the positive semi-axis of normal stresses have been termed the crack propagation steps of second stage. They are all collected in Fig. 9, together with the last circle of first stage. The stress analysis for an intermediate and the last step of crack propagation in the second stage are shown, respectively, in Fig. 10 and Fig. 11.

As regards the Mohr's pole, in Fig. 9 we can notice a progressive anti-clockwise rotation as the crack propagates. For the propagation steps successive to the first, speaking of tangent point is not appropriate, since the circle is no longer tangent but secant or external to the limit domain. As limit point to consider together with the Mohr's pole for defining the crack propagation direction, the point lying furthest outside the limit domain has been chosen. This point is marked in Fig. 9 for each Mohr's circle. Since the Coulomb criterion has been chosen as failure criterion, the limit domain is represented by two lines in the Mohr-Coulomb plane. Thus, the central angle de-

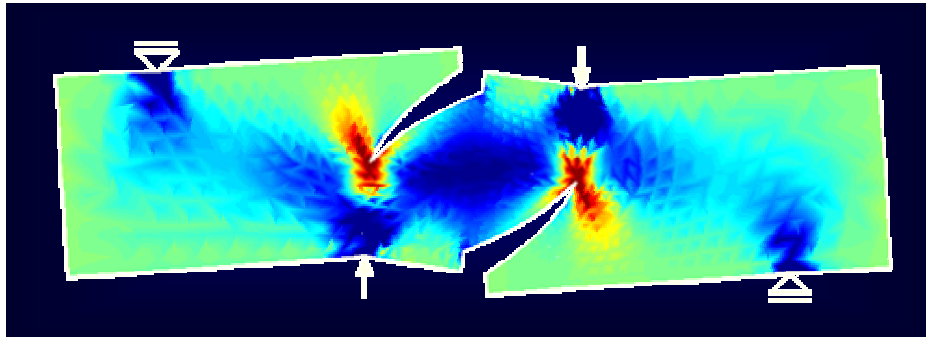


**Figure 11** : Stress analysis at the end of the second stage

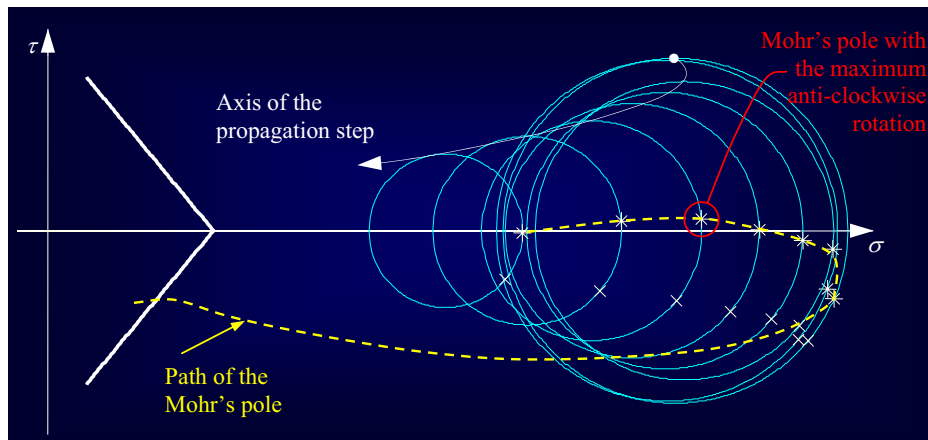


**Figure 12** : Mohr's circles for tip stress analysis in the third stage of the carrying process

scribing the position of the limit point with respect to the positive semi-axis of normal stresses is the same for each circle. Due to Mohr's pole rotation, the propagation direction following from these limit points turned out to be progressively increasing for all propagation steps of the second stage (Fig. 11).

At the end of the second stage, the Mohr's circle has reached its maximum radius and positive shifting. From this moment forth, the circle becomes smaller and smaller as the crack propagates. Moreover, the circle begins to move along the negative verse of the normal stress axis. All circles of this further stage of the carrying process, the third stage, are collected in Fig. 12, together with the last circle of second stage.

The inversion of tendency which characterizes the third stage does not follow from a crack propagating in order to approach a new stable condition. It is caused by the beam downloading, following from the advanced state of crack

propagation. It must be recalled, in fact, that the simulation is performed in displacement-control. For impressed displacements smaller than the displacement of crack initiation, increasing of applied load follows from increasing of impressed displacement. As the crack begins to propagate, the beam stiffness begins to decrease. This modifies the relationship between impressed displacement and applied load. When the stiffness decreasing is above a certain limit value, increasing of impressed displacement is accompanied by decreasing of applied load. Finally, if the decrease of applied load is consistent, the stress field at crack tip vanishes as the crack propagates at constant value of impressed displacement. This is what actually happens in the third stage of the carrying process.

In the third stage, the total rotation of the Mohr's pole reaches its maximum anti-clockwise value (Fig. 12). For the last steps of propagation, the Mohr's pole rotates in

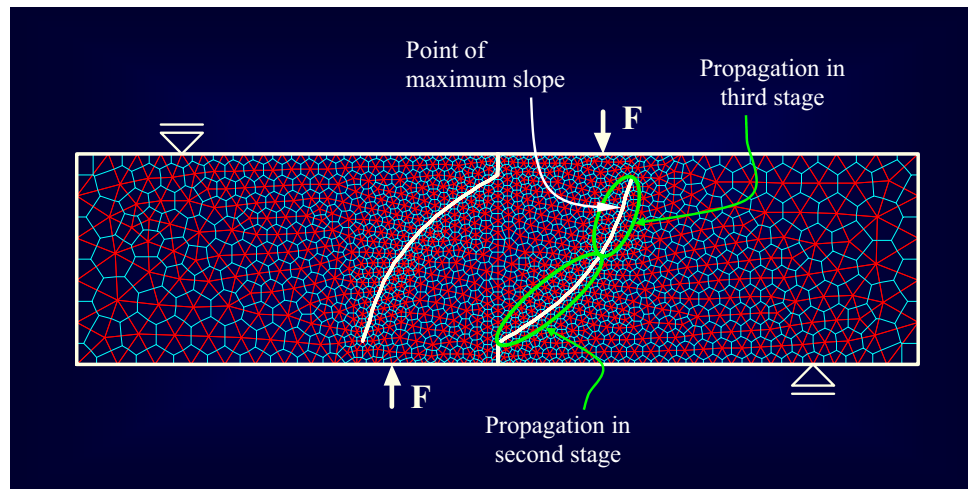


**Figure 13** : Complete crack path for the second and third stage

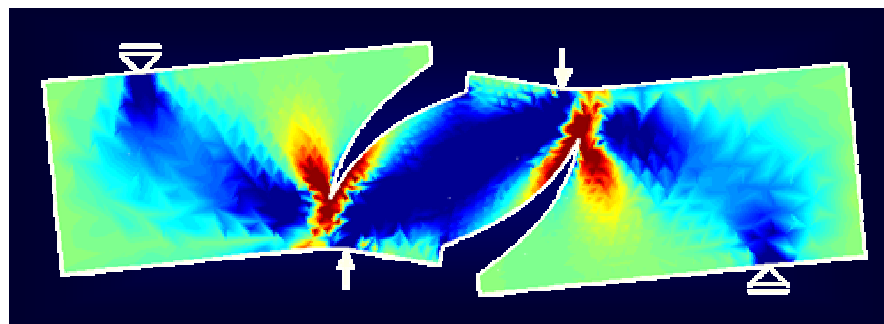


**Figure 14** : Interaction between tip stress field and punching zone for the point with the maximum slope of the crack path

clockwise sense, leading to a propagation direction decreasing with crack propagation (Fig. 13). The crack path following from this inversion of rotation is characterized by a tip moving toward the applied load until the tip reaches the punching zone under the applied load (Fig. 14). From this moment forth, interaction between the stress field into the punching zone (compressive stresses) and around the tip (tensile stresses) leads the tip to deviate from its trajectory (Fig. 13). Orientation and deviation of the crack path are confirmed by the experimental evidence.

The last Mohr's circle in Fig. 12 represents the tip stress analysis for the crack path in Fig. 15. At this point, the beam was considered as completely cracked and the simulation stopped.

Stage two and three completely describe the stress field

at crack tip for the crack path which activates at the displacement of crack initiation. The beam fails in brittle manner for the displacement of crack initiation, since each step of crack propagation leads to an unstable crack path.

#### 4.2 Example of Non-Brittle Crack: The Lok-Test

We are faced with a non-brittle crack whenever the crack path develops in such a way as to lead the crack into a new stable configuration. In a displacement-controlled numerical simulation with fixed length of crack propagation, this means that several crack propagations occur for the same value of impressed displacement before a stable condition is reached. In the flow-chart in Fig. 1.a, for use with the CM, a non-brittle failure involves reaching crack stabilization a number of times before crushing.

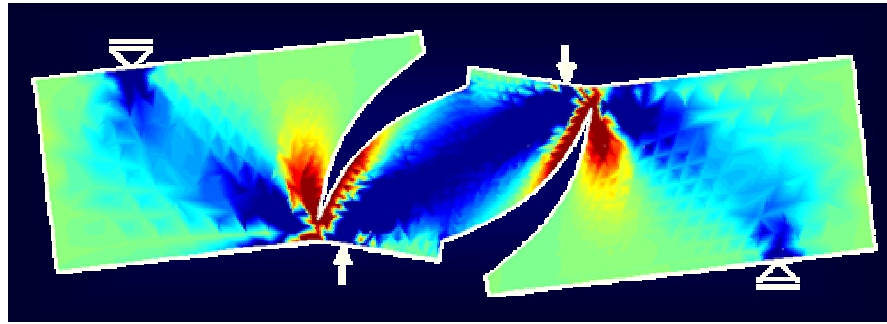


Figure 15 : Stress analysis at the end of the third stage

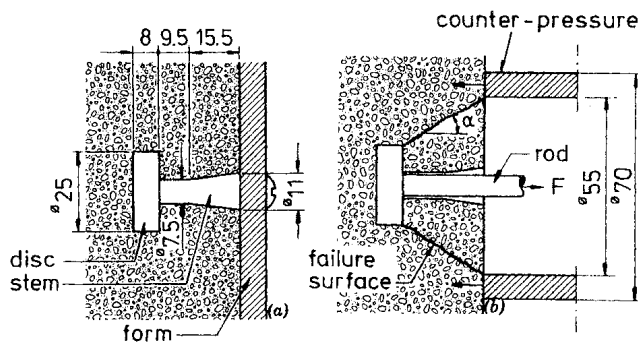


Figure 16 : Application and configuration of Lok-Test (all dimensions are in millimeters)

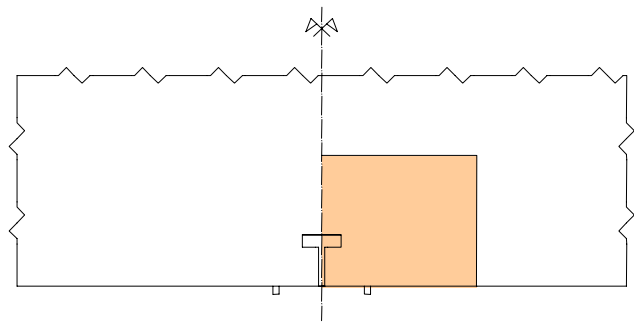


Figure 17 : Geometry to model and stress extinction zone of the load transferred by the steel insert

Thus, further increments of impressed displacement are possible after having reached the displacement of crack initiation.

As an example of non-brittle crack, consider the pullout test on a concrete specimen. The test apparatus and procedure for the Danish version of the pullout test, the Lok-Test, are illustrated in Fig. 16 [Ottosen (1981)].

In Fig. 17, the modeled domain is shown for the case of Lok-test simulation [Ferretti (2003b)]. It corresponds to the stress extinction zone of the load transferred by the steel insert. Mohr's circle for the limit condition involving the first crack propagation is depicted in Fig. 18. Also the two tangent points and the two propagation directions are depicted in Fig. 18. Fig. 18 is equivalent to Fig. 4 except for the limit surface since, this second time, the Leon criterion was used. The Leon criterion is quite adequate for describing the direction of propagation both in the compressive and in the tensile field. It can be considered a refinement of the Coulomb criterion, previously used.

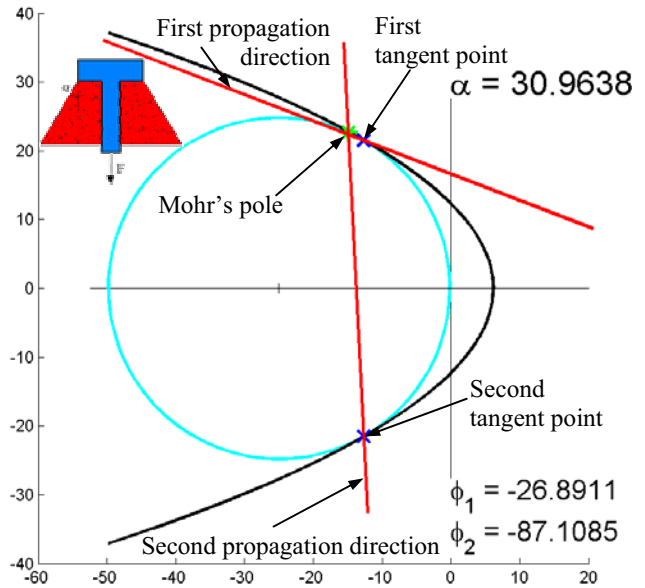
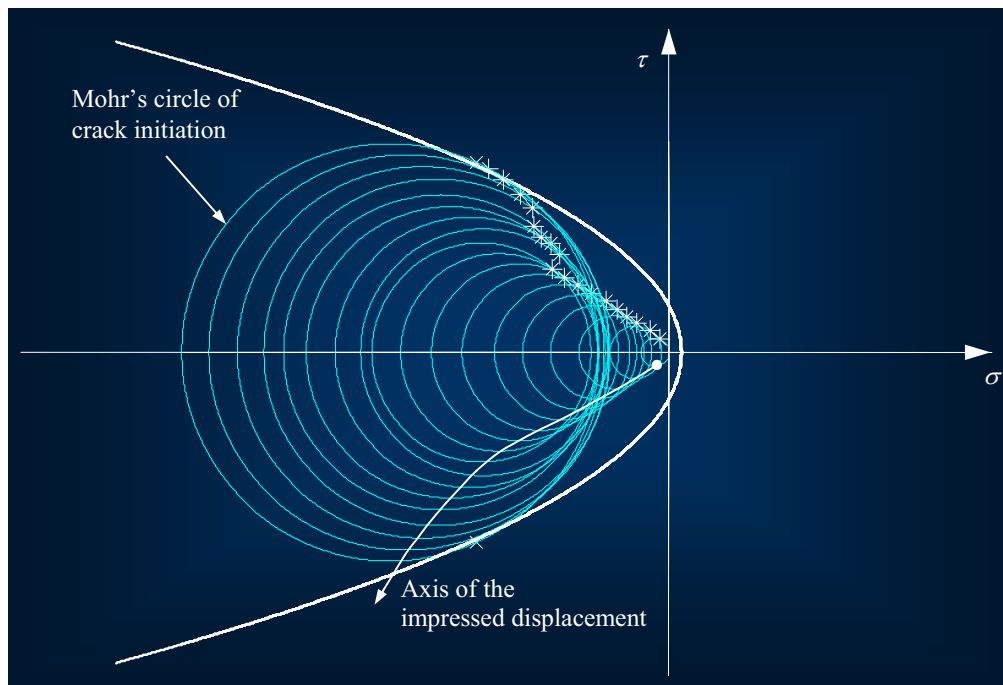


Figure 18 : Limit condition and directions of first propagation for the geometry of the Lok-Test



**Figure 19** : Mohr's circles for tip stress analysis in the first stage of the carrying process

In accordance with Fig. 16, the initiation point is at the bottom right corner of the disc stem in Fig. 17. At the limit condition, both the cracks along the first and the second propagation direction of Fig. 18 propagate from the bottom right corner toward the counterpressure ring. More precisely, the first propagation direction runs above the counterpressure ring and the second propagation direction runs below the counterpressure ring, resulting in the same constraint degree along the two directions. Thus, both cracks enucleate on the bottom right corner as the limit condition is reached. This is in good agreement with the experimental evidence [Krenchel and Bickley (1985)]. Nevertheless, from the experimental evidence [Krenchel and Bickley (1985)], it is also known that the crack along the first propagation direction stops propagating after a few propagation steps, due to the interaction between the stress fields at the two crack tips. Thus, only one failure surface is observed experimentally, the one corresponding to the second propagation direction. This is why only propagation along the second direction has been considered when updating the modeled domain. As in the case of brittle failure simulation, the analysis of crack propagation was performed in displacement-control (Fig. 1.a). This second time too, from the value

of impressed displacement equal to zero up to the displacement of crack initiation, the failure condition was never reached. Thus, the value of impressed displacement can be incremented, going out from the gray-filled cycle in Fig. 1.a. The tip stress analysis in the Mohr's plane from the zero displacement up to the condition of crack initiation (first stage of the carrying process) is shown in Fig. 19. The biggest circle in Fig. 19 intersects the limit domain, involving crack propagation along the two directions individuated by Mohr's pole and tangent points. Geometry updating is then activated, letting the crack propagate along the second direction of propagation. The new tip stress analysis following from this updating returns the smaller of the circles in Fig. 20. This circle is internal to the limit domain, stating that the crack configuration is stable for the displacement of crack initiation. The condition for going out of the gray-filled cycle in Fig. 1.a is thus reached, and further displacement increments can occur (second stage of the carrying process). The circle following from the first increment of impressed displacement is still internal to the limit domain (Fig. 20). Thus, the crack configuration is still stable. Two increments of impressed displacement are needed in order to activate a new crack propagation (Fig. 20).

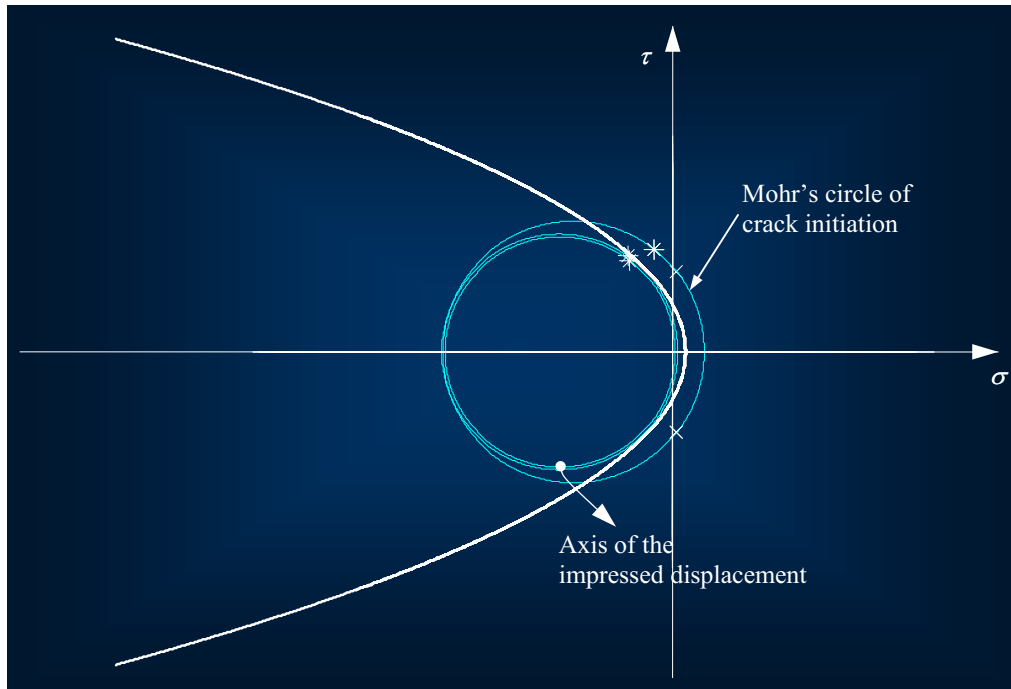


**Figure 20** : Mohr's circles for tip stress analysis in the second stage of the carrying process

Also for this new crack propagation, the crack path develops in such a way as to reach a new stable configuration. The last circle of second stage, the one activating the new propagation, is depicted in Fig. 21 together with Mohr's circles corresponding to each of the propagation steps leading to the new crack stabilization. As can be appreciated from Fig. 21, after seven steps of propagation at the same value of impressed displacement, Mohr's circle re-enters into the limit domain and the crack stabilizes. The circle for which the crack is stable is depicted in Fig. 21 in thick line.

The value of impressed displacement is then incremented (third stage of the carrying process). A further crack propagation was found to occur for this last value of impressed displacement, since the corresponding tip stress analysis involves a circle intersecting the limit surface. This circle has been plotted in Fig. 22 together with the circle involving stabilization in the second stage of the carrying process.

This last time too, the failure which has activated is non-brittle, and a stable configuration is reached after two propagations. The circle of third stage re-activating crack propagation is depicted in Fig. 23 together with Mohr's circles corresponding to the propagations steps after the

third stage.

In Fig. 23, the circle involving crack stabilization is depicted in thick line. Once the crack has stabilized, the impressed displacement has been incremented, giving a Mohr's circle intersecting the limit domain. This circle has been plotted in Fig. 24 brought together with the circle in thick line of Fig. 23.

Stabilization for this value of impressed displacement is not possible, and the cracks which subsequently activate are brittle. As can be appreciated in Fig. 25, indeed, from this moment forth, crack propagation does not involve circles approaching the limit surface, and the stable condition can no longer be reached. This crack thus propagates until crushing, for the same value of impressed displacement.

In Fig. 25 one can also see how, during the brittle crack propagation, the failure mechanism changes from shear-compression to shear-tension and pure tension, since the limit point passes from the negative to the positive semi-plane of normal stresses.

The final crack path and stress analysis are shown in Fig. 26. As can be seen by comparison between Fig. 26 and Fig. 27, the numerical crack path is in good agreement with the trumpet shaped failure surface which has been

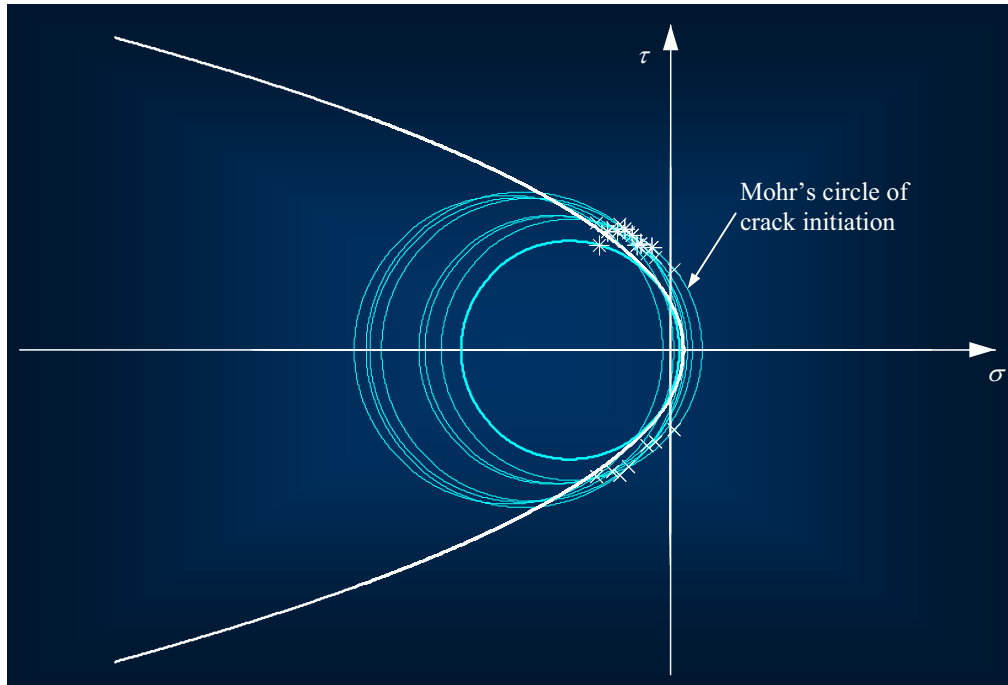


Figure 21 : Mohr's circles for tip stress analysis during the second crack propagation

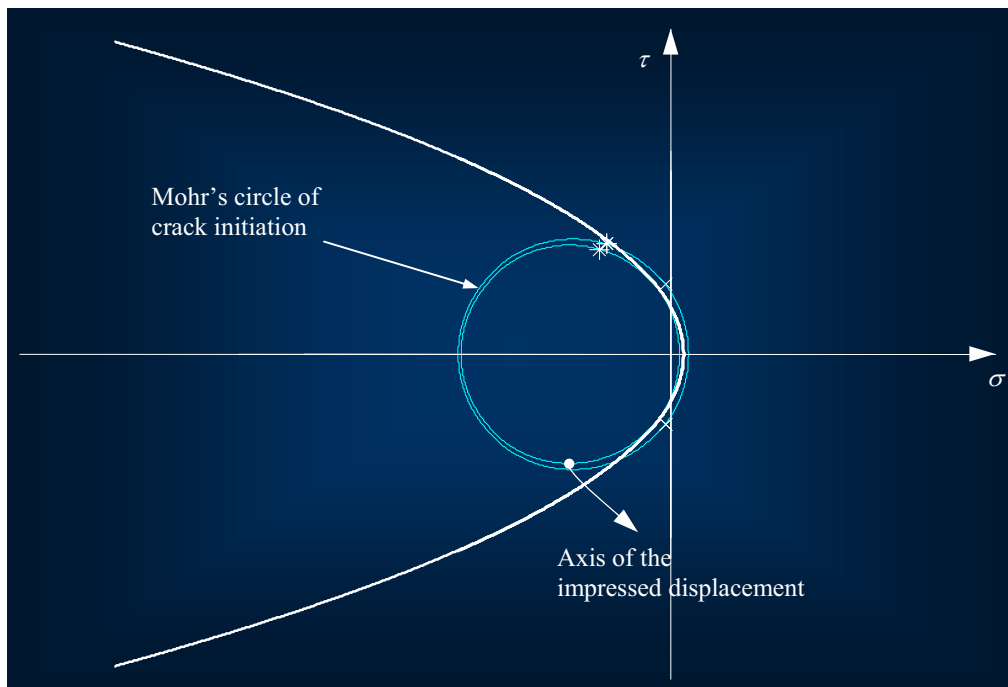


Figure 22 : Mohr's circles for tip stress analysis in the third stage of the carrying process

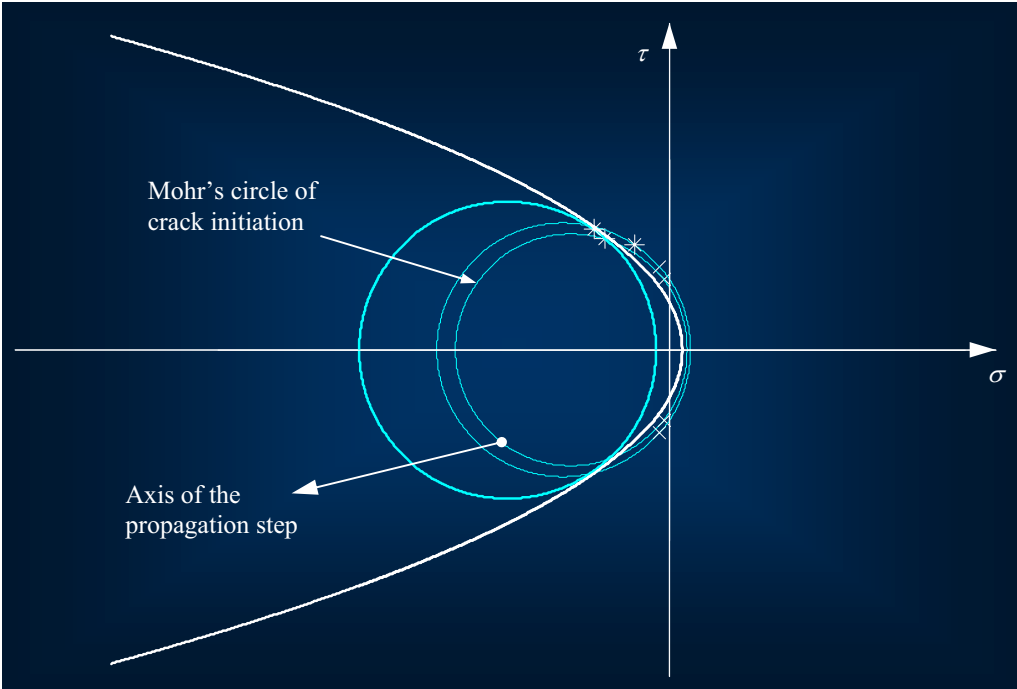


Figure 23 : Mohr's circles for tip stress analysis during the third crack propagation

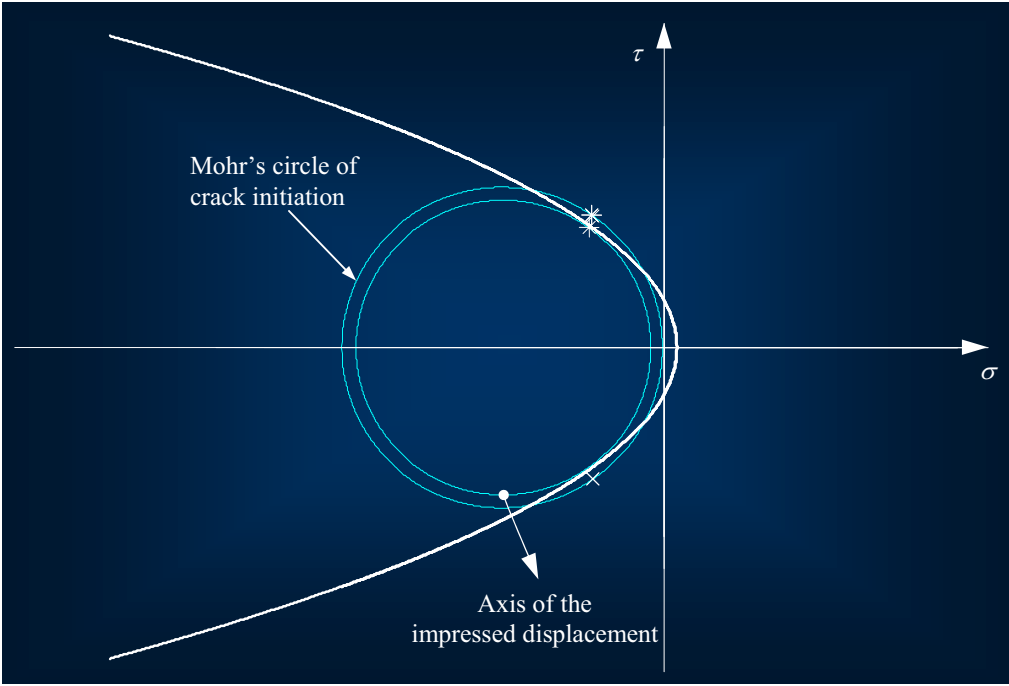


Figure 24 : Mohr's circles for tip stress analysis in the fourth stage of the carrying process

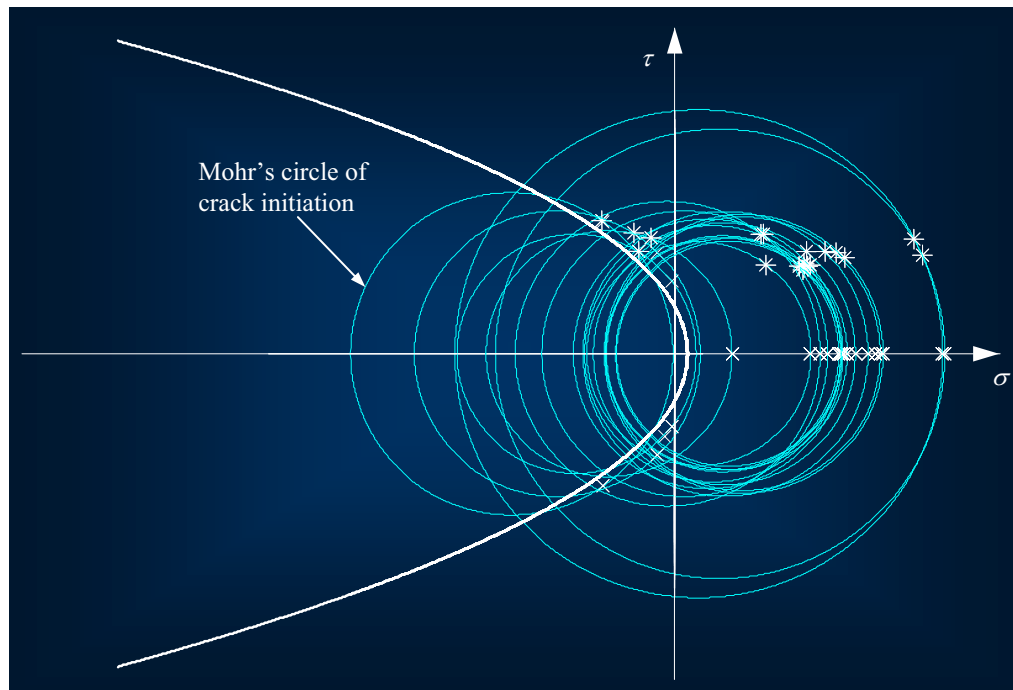


Figure 25 : Mohr's circles for tip stress analysis during the fourth crack propagation

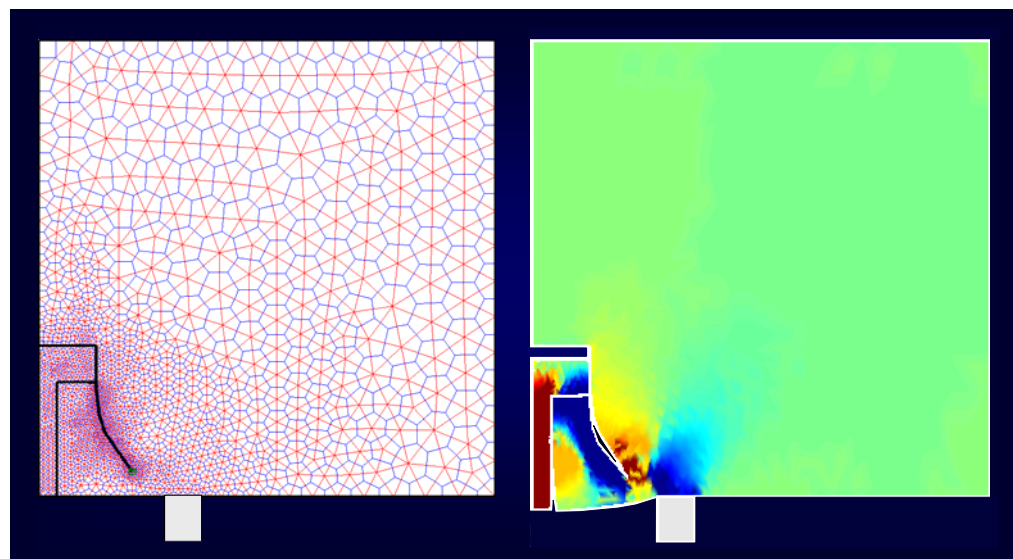
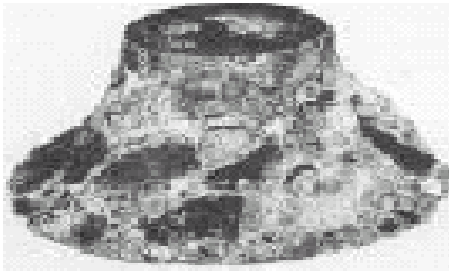


Figure 26 : final crack path and stress analysis on the deformed configuration



**Figure 27** : Shape of the extracted concrete portion

found experimentally [Yener and Chen (1984), Krenchel and Bickley (1985)].

## 5 Conclusions

Numerical results have been presented for propagation of brittle and non-brittle cracks. The complete crack path has been derived by means of the Cell Method (CM) and a nodal relaxation with remeshing technique.

The CM with nodal relaxation and remeshing technique is a discrete method, which stands as an alternate approach to the use of the differential formulation for crack propagation analysis [Han and Atluri (2002), Han and Atluri (2003), Nishioka et al. (2002)]. The use of the CM allows us to treat punctual forces easily. Thus, the punching effect can be studied easily as well. Moreover, a finite value of stress was found in the neighborhood of the crack tip, due to the direct discrete approach which is the base of the CM. That is, the stress around the crack tip does not approach infinity as the crack tip is approached. This represents the physical nature of the problem, since the  $1/\sqrt{r}$  singularity at the crack tip is based on the hypothesis of an idealized elastic material [Muskhelishvili (1953), Westergaard (1939)].

It has been shown how an adequate choice of the propagation length together with an iterative updating procedure allow an accurate description of the crack path in brittle propagation. Thus, the problem of defining the crack geometry at various moments in time during a static propagation can be easily solved numerically. The geometry of the crack is not prescribed, but identified iteratively through crack stability analysis. In particular, the direction of crack propagation is iteratively computed, taking into account stress field modifications induced by crack propagation. A polygonal crack path

is then derived, in good accordance with the experimental evidence. The iterative stress analysis on the crack tip leads to considering interactions between stress fields of opposite signs as the crack propagates. Implications on the propagation direction of these interactions are automatically taken into account by the tool of geometry updating. The resulting numerical crack path is characterized by trajectory deviation as the tip stress field interacts with compressed zones. Trajectory deviation has been shown in the case of beam in four point bending.

The analysis of crack stability has been performed in the Mohr's plane. In this plane, brittle cracks are characterized by Mohr's circles going away from the limit domain. On the contrary, non-brittle cracks are characterized by Mohr's circles approaching the limit domain after few steps of crack propagation. Mohr's circle path during failure at constant displacement is here provided both for the case of brittle and non-brittle crack. The analysis in the plane of Mohr also allows evaluation of the modification of the failure mechanism with crack propagation. An example of failure mechanism evaluation is provided here for the Lok-test simulation. This evaluation is all the more relevant as defining the actual failure mechanism in a Lok-test is an open problem, nowadays. No FEM code developed in the past is decisive in solving this problem [Yener (1994), Ferretti (2003b)].

**Acknowledgement:** All the results here presented are part of the CIMEST Scientific Research on the Identification of Materials and Structures – DISTART – Faculty of Engineering – Alma Mater Studiorum of Bologna.

## References

- Bouchard, P. O.; Bay, F.; Chastel, Y.; Toven, I.** (2000): Crack Propagation Modelling using an Advanced Remeshing Technique. *Comput Methods Appl Mech Engrg*, vol. 189, pp. 723-742. Elsevier.
- Buliga, M.** (1999): Energy Minimizing Brittle Crack Propagation. *J. of Elasticity*, vol. 52, No. 3, pp. 201-238.
- Cosmi, F.** (2000): Applicazione del Metodo delle Celle con Approssimazione Quadratica. *Proc AIAS 2000*, pp. 131-140.
- Fenner, R. T.** (1996): *Finite Element Methods for Engineers*. Imperial College Press, London.
- Ferretti, E.** (2001): *Modellazione del Comportamento*

- del Solido Cilindrico Compresso*. Ph.D. Thesis, University of Lecce, Italy.
- Ferretti, E.** (2003a): Crack Propagation Modeling by Remeshing Using the Cell Method (CM). *CMES: Computer Modeling in Engineering & Sciences*, vol. 4, No. 1, pp. 51-72.
- Ferretti, E.** (2003b): A Cell Method (CM) Code for Modeling the Pullout Test Step-wise. *CMES: Computer Modeling in Engineering & Sciences*, submitted.
- George, P. L.** (1995): Automatic mesh generator using the Delaunay Voronoi principle. *Surv. Math. Ind.*, pp. 239-247.
- Han, Z. D.; Atluri, S. N.** (2002): SGBEM (for Cracked Local Subdomain) – FEM (for Uncracked Global Structure) Alternating Method for Analyzing 3D Surface Cracks and Their Fatigue-Growth. *CMES: Computer Modeling in Engineering & Sciences*, vol. 3, No. 6, pp. 699-716.
- Han, Z. D.; Atluri, S. N.** (2003): Truly Meshless Local Petrov-Galerkin (MLPG) Solutions of Traction & Displacement BIEs. *CMES: Computer Modeling in Engineering & Sciences*, vol. 4, No. 6, pp. 665-678.
- Har, J.** (1998): *A New Scalable Parallel Finite Element Approach for Contact-Impact Problems*. Ph.D. Thesis, Georgia Institute of Technology, Atlanta.
- Hirsch, P. B.; Booth, A. S.; Ellis, M.; Roberts, S. G.** (1992): Dislocation-driven Stable Crack Growth by Microcleavage in Semi-brittle Crystals. *Scripta Metall et Mater.* vol. 27, pp. 1723-1728.
- Holian, B. L.; Blumenfeld, R.; Gumbsch, P.** (1997): An Einstein Model of Brittle Crack Propagation. *Physical Review Letters*, vol. 78, No. 1, pp. 78-81.
- Huebner, K. H.** (1975): *The Finite Element Method for Engineers*. Wiley.
- Krenchel, H.; Bickley, J. A.** (1985): Pullout Testing of Concrete. Historical Background and Scientific Level Today. *Nordic Concrete Research*, Publ. No. 6, The Nordic Concrete Federation.
- Kysar, W.** (2001): Continuum simulations of directional dependence of crack growth along a copper / sapphire bicrystal interface. Part II: crack tip stress / deformation analysis. *Journal of the Mechanics and Physics of Solids*, vol. 49, pp. 1129-1153.
- Livesley, R. K.** (1983): *Finite Elements, an Introduction for Engineers*. Cambridge University Press.
- Machida, S.; Aihara, S.** (1996): Computer Simulation of Brittle Crack Propagation and Arrest of Steel Plate with Temperature Gradient Based on Local Fracture Stress Criterion. *ASTM, Fracture Mechanics Symp.*, Saratoga Sprig, N.Y.
- Muskhelishvili, N. I.** (1953): *Some Basic Problems on the Mathematical Theory of Elasticity*. Noordhoff-Groningen.
- Nishioka, T.; Furutuka, J.; Tchouikov, S.; Fujimoto, T.** (2002): Generation-Phase Simulation of Dynamic Crack Bifurcation Phenomenon Using Moving Finite Element Method Based on Delaunay Automatic Triangulation. *CMES: Computer Modeling in Engineering & Sciences*, vol. 3, No. 1, pp. 129-146.
- Ohtsuka, K.** (2000): Theoretical and numerical analysis on brittle fracture in 2D and 3D cases. *International Symposium on Mathematical Modeling and Numerical Simulation in Continuum Mechanics*, Pal-Lu-Plaza Yamaguchi.
- Ottosen, N. S.** (1981): Nonlinear Finite Element Analysis of Pull-Out Test. *Journal of the Structural Division*, vol. 107, No. ST4, pp. 591-603.
- Papadopoulos, P.; Jones, R. E.; Solberg J.** (1995): A Novel Finite Element Formulation for Frictionless Contact Problems. *Int J Num Meth Engrg*, vol. 38, pp. 2603-2617.
- Stumpf, H.; Le, K. C.** (1990): Variational principles of nonlinear fracture mechanics. *Acta Mechanica*, vol. 83, pp 25-37.
- Tonti, E.** (2001): A Direct Discrete Formulation of Field Laws: the Cell Method. *CMES: Computer Modeling in Engineering & Sciences*, vol. 2, No. 2, pp. 237-258.
- Westergaard, H. M.** (1939): Bearing Pressures and Cracks. *J Appl Mech*, vol. 6, pp. 49-53.
- Yener, M.** (1994): Overview and Progressive Finite Element Analysis of Pullout Tests. *ACI Structural Journal*, vol. 91, No. 1, pp. 49-58.
- Yener, M.; Chen, W. F.** (1984): On In-Place Strength of Concrete and Pullout tests. *Journal of Cement, Concrete, and Aggregates*, vol. 6, No. 2, pp. 90-99.
- Zhong, Z. H.** (1993): Finite Element Procedures for Contact-Impact Problems. Oxford/New York/Tokyo, 372 pp., Book review: *Appl. Mech. Rev.*, vol. 48, No. 5, 1995, 5R4 (written by M Okrouhlik).